Title

Interaction of Hydrogen with MB6 (M = Ba, Ca, La, and Sr) Surfaces from First Principles

Journal

ACS Omega, 4(1)

ISSN

2470-1343

Authors

Schmidt, Kevin M
Misture, Scott T
Graeve, Olivia A
et al.

Publication Date

2019-01-31

DOI

10.1021/acsomega.8b02652

Peer reviewed

ACS OMEGA

Article

Cite This: ACS Omega 2019, 4, 65−72

http://pubs.acs.org/journal/acsodf

Interaction of Hydrogen with MB_6 (M = Ba, Ca, La, and Sr) Surfaces from First Principles

Kevin M. Schmidt,[†] Scott T. Misture,[‡] Olivia A. Graeve,[§] and Victor R. Vasquez*[,†]

[†]Chemical and Materials Engineering Department; University of Nevada Reno; Reno, Nevada 89557, United States

[‡]Kazuo Inamori School of Engineering; Alfred University; 2 Pine Street; Alfred, New York 14802, United States

[§]Department of Mechanical and Aerospace Engineering; University of California, San Diego; La Jolla, California 92093, United States

ABSTRACT: We show results of basic energetics and interacting behavior of hydrogen with metal hexaboride surfaces using a combination of self-consistent density functional calculations and dynamics based on the Car−Parrinello method. Our results show that hydrogen is strongly attracted to localized exposed boron atoms and interactions with the terminal cations are strictly repulsive. From these, preliminary local adsorption energy calculations suggest that a single hydrogen molecule per surface unit-cell is possible (one ML). Strongest bonds are found when hydrogen is above the terminal boron atoms affected by reduced coordination and dangling bonds. This location serves to restore the hexaboride unit to a more stable structure by providing electronic density to the deficient surface octahedra. Additionally, trajectories from dynamic simulations provide insight into how hydrogen recombination reactions occur on the surface through dissociative adsorption and the method of travel prior to recombination to be along the octahedral face and bridging sites connecting separate unit cells on the surface. Upon adsorption, a single hydrogen atom becomes localized at the dangling bond site while the second interacts with the surface along a weaker potential energy path. Desorption at lower temperatures occurs when migrating atoms from separate adsorption sites intersect to form a new pair.

1. INTRODUCTION

Metal hexaboride (MB_6) materials are commonly used as cathodes in electron optical instruments owing to their low work functions and low evaporation rates.[1] Experimental and theoretical studies investigating adsorption on MB_6 surfaces have mainly focused on determining the poisoning effects on the emitter planes caused by common environmental gases such as CO, O_2, and H_2O.[2−13] Although hydrogen is considered a background gas in ultrahigh vacuum conditions,[14] only a handful of studies consider the interaction of hydrogen with MB_6 surfaces and theoretical investigations are absent from the literature to the best of our knowledge. Most experimental, modeling, and theoretical efforts are focused on electronic behavior and thermophysical properties for bulk MB_6 materials.[15−21]

Buckingham[22] sought to determine the effects related to environmental gases, including hydrogen, on the performance of thermionic cathodes. In contrast with a majority of the electronegative atmospheric compounds tested, a positive effect was observed—the background hydrogen was found to improve the performance of poorly activated cathodes (those requiring work to promote lanthanum coverage at the emitter tip). Nagaki et al.[23] performed a thorough analysis quantifying the hydrogen−deuterium recombination reaction using a LaB_6 catalyst, suggesting that exposed terminal boron atoms were probable active sites for this equilibration reaction. This conclusion was supported by the relatively low turnover rate and generally accepted hypothesis that most MB_6 are metal-terminated. Note that the catalytic H−B interaction on LaB_6 surfaces parallels the cathode improvement observed by Buckingham, as excess metal on the surface is generally associated with lower work functions.[24] In more current research, MB_6 materials are being investigated as a transient product in hydrogenation reactions for reversible hydrogen storage.[25]

Although the experimental publications considering the nature of interactions between hydrogen and MB_6 materials are very limited in number, each one provides a distinct piece of evidence to allow for comparison with in silico results. We continue the research effort by studying energetics, bonding geometries, surface modifications, and electronic changes associated with hydrogen interactions at different sites on four MB_6 materials. We restrict our focus to the (001) surfaces of MB_6 using stoichiometric slab supercells. At this point, it is unclear which surface would be most suitable for the analysis, as most experimental work is unclear on the surface terminations on metal hexaborides. In agreement with Nagaki et al.,[23] we find that hydrogen adsorption is only possible on MB_6 structures presenting accessible boron atoms, with binding energies as low as −2.316 eV/H. Additionally, we provide evidence for a possible mechanism explaining the H_2−D_2 equilibration reported more than 35 years ago.

2. THEORETICAL METHODS

2.1. Surface Geometries. The bulk unit cell of metal hexaborides is simple cubic with space group $Pm\bar{3}m$ symmetry. A single metal atom is found on the origin along with six boron atoms, forming an octahedral unit, whose barycenter is at the

Received: October 4, 2018
Accepted: December 21, 2018
Published: January 2, 2019

DOI: 10.1021/acsomega.8b02652
ACS Omega 2019, 4, 65−72

(1/2, 1/2, 1/2) location of the unit cell. The lattice can be fully described using only the lattice constant, a, and positional parameter, z, as shown in Figure 1. To describe the (100)

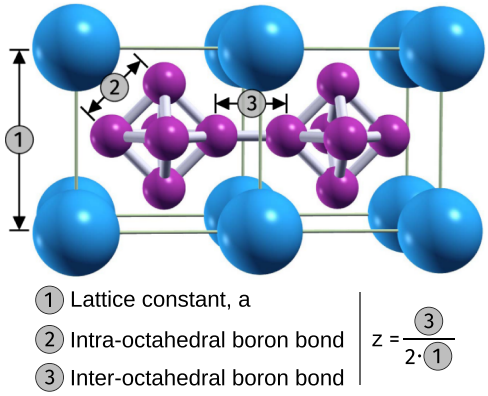

Figure 1. Metal hexaboride structure showing relevant bond lengths. Each unit cell contains one cation (blue) and six boron atoms (purple) forming an octahedral structure. The positional parameter, z, is defined as half the interoctahedral bond distance divided by the lattice constant, a.

surfaces, we use four stoichiometric slabs resulting from a previous study[26] on the stability of various MB_6 terminations. Three of the surfaces have repeating units which have a depth of one unit-cell along the x-direction, shown in Figure 2 as

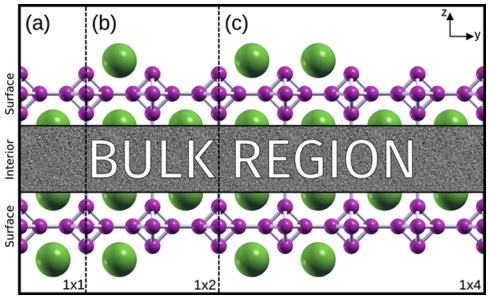

Figure 2. Slice of a stoichiometric slab displaying (a) polar 1 × 1 and symmetric (b) 1 × 2 and (c) 1 × 4 hypothetical surfaces. Each surface of the slab, shown as the portion outside of the bulk region, repeats in the x-direction with a single unit-cell periodicity.

two-dimensional slices through a slab model. The polar 1 × 1 surface in Figure 2a consists of separate cation-terminated and boron-terminated faces and is used as a baseline for comparison. Notice that this surface configuration is ideal in the sense that it shows a complete segregation of boron and metal ions in a symmetric fashion, but because it is polar, the metal hexaboride will essentially be in layers of alternating planes of opposite charge causing what is known as a polar catastrophe. The electrostatic potential increases with thickness piling up bulk dipole moments and causing electrostatic divergence. Electrostatic stability is achieved by surface reconstruction or reorganization of atoms with charge redistribution accordingly. In other words, other surface arrangements occur to stabilize the surface. These however are found to produce the lowest surface energy through electronic structure calculations at 0 K for alkaline-earth hexaborides.[26] The 1 × 2 and 1 × 4 surfaces depicted in Figure 2b,c, respectively, terminate with alternating rows of cations and vacancies, and the 1 × 2 structure has been observed experimentally on freshly cleaved CaB_6 single crystals using low-energy electron diffraction.[27] The fourth geometry considered has a two-dimensional repeating unit along the surface plane, and Figure 3 provides two different perspectives

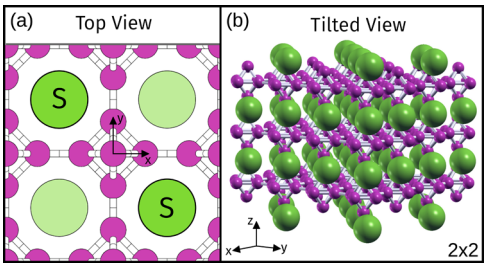

Figure 3. Geometry of the 2 × 2 slabs. (a) Surface cations, S, viewed from above the (001) face. Faded circles represent metals below the first layer of boron atoms. (b) Diagonal rows of terminal cations shown from the side of a small slab supercell.

for the 2 × 2 slab. Looking down from the top of the crystal in Figure 3a, a checkerboard pattern is formed by the surface cations (labeled S). Figure 3b shows a space-filling model of a three-layer slab after a slight rotation, where parallel rows formed along the diagonals can be seen.

Each slab supercell is constructed to contain 15 layers along the surface normal, and atoms located in the central cells are constrained to their equilibrium positions during ionic relaxation to act as a bulk reservoir. As previously established,[26] the chosen layer depth has shown to produce converged results for surface energies and coordinate relaxations,[26] generating surface energies with standard deviations less than 0.05% using several converged layer counts. Another important parameter which can substantially alter the results from electronic structure calculations is the vacuum size between slab supercells. We separate each surface with a vacuum length of 25.46 Å for BaB_6 (4.2437), 24.87 Å for CaB_6 (4.1445), 24.90 Å for LaB_6 (4.1501), and 25.16 Å for SrB_6 (4.1935), respectively, making the overall distance along the z-direction equivalent to a total of 21 bulk unit-cell lengths for each system. The values in parentheses are the unit cell size of each metal hexaborides in angstroms. Calculated local adsorption energies, work functions, and bond lengths are converged to less than 1 meV and 1 pm, respectively. Additionally, dipole corrections[28] are implemented with the capacitor placed directly in the center of the vacuum. For a more comprehensive adsorption study of hydrogen in these materials, one would have to consider the extent of adsorption coverage by the hydrogen, which is not part of this work. Additionally, larger supercells are more appropriate to include deformations, defects, and grain boundaries among other phenomena, but the computational costs with ab initio-based methods can quickly become prohibitive. In this work, we focus on providing insights on the hydrogen interactions on MB_6 materials for Ba, Ca, La, and Sr to identify the potential of the materials for new applications, such as hydrogen storage, by understanding local mechanisms of interaction.

2.2. Density Functional Theory. Electronic structure calculations, within density functional theory (DFT), are performed using the integrated suite of open-source computer codes, QUANTUM ESPRESSO,[29] based upon plane waves and pseudopotentials. Exchange and correlation effects are described by the Perdew−Burke−Ernzerhof functional[30]

DOI: 10.1021/acsomega.8b02652
ACS Omega 2019, 4, 65−72

within the generalized gradient approximation. A Monkhorst–Pack set of special k-points[31] and Marzari–Vanderbilt cold smearing[32] are used to integrate over the Brillouin-zone.

Ultrasoft pseudopotentials generated through the Vanderbilt scheme[33] with nonlinear core corrections are used to represent the interactions between the ionic core and valence electrons for all atoms in this work.[29] Each of the alkaline earth metals has 10 valence electrons with $3s^2 3p^6 3d^0 4s^2$, $4s^2 4p^6 4d^1 5s^1 5p^0$, and $5s^2 5p^6 5d^0 6s^2 6p^0$ configurations for atoms Ca, Sr, and Ba, respectively. Lanthanum contains 11 electrons in its valence with a $5s^2 5p^6 5d^1 6s^{1.5} 6p^{0.5}$ configuration, and the boron pseudopotential has three valence electrons in a $2s^2 2p^1$ configuration. Kinetic energy cutoffs for the plane wave basis are 30 Ry for the wave function and 400 Ry for the charge density for all systems, and these values are converged to 1 mRy/atom using a bulk unit cell energy calculation. Smearing widths and k-points for each crystal are determined by monitoring atomic forces after a 10% displacement of the metal cation in the lattice and selecting values which agree within 0.001 eV/Å/atom for a dense mesh of k-points ($24 \times 24 \times 24$) and low smearing width (1 mRy). Unit cells for the divalent metal hexaboride systems use a $6 \times 6 \times 6$ k-point mesh and smearing widths of $\sigma_{Ca} = 5$ mRy, $\sigma_{Sr} = 5$ mRy, and $\sigma_{Ba} = 10$ mRy. In contrast to the alkaline-earth hexaborides in this study, lanthanum hexaboride is a metallic conductor and requires a set of parameters more suitable for self-convergence. For LaB_6, we use an $8 \times 8 \times 8$ k-point mesh for the unit cell along with $\sigma_{La} = 20$ mRy for electron smearing. These parameters have been previously tested[26] and show good agreement with reported experimental values in the literature, achieving deviations less than 0.5 and 0.2% for calculated lattice constants and positional parameters, respectively. Additionally, bulk moduli are also in good agreement with published results.

2.3. Car–Parrinello Dynamics. In an effort to reduce the search space for preferential binding locations, we perform molecular dynamics simulations using the Car–Parrinello scheme[34] (CPMD) within DFT. The equations of motion are integrated with a time step of 7.5×10^{-17} s over the course of 10^5 steps at a temperature of $T = 50$ K. Wavefunction and charge density cutoffs are identical to those for self-consistent field calculations. We find that an effective electron mass of 200 au (0.10972 amu) and kinetic energy cutoff of 3 Ry are sufficient to maintain adiabicity and model the system accurately.

Supercells for CPMD simulations are constructed to have nine unit cells along the surface normal (z-direction), comprising a five-layer slab along with four layers of vacuum. Additionally, a minimum of two unit cell widths is given along the x- and y-directions to mitigate interactions between neighboring images. Because of the polar nature of the 1×1 slabs, both boron-terminated and metal-terminated surfaces are studied. Additionally, boron-terminated slabs require the use of passivation on the "bulk" side to deter H_2 molecules from interacting with these surfaces. For these, we place a single hydrogen atom atop each of the terminal boron atoms per unit cell. Slabs having 1×2, 2×2, and 1×4 terminations are symmetric by construction and are therefore simulated without further modification. We perform two sets of simulations for each slab with two and eight hydrogen molecules added to the vacuum space.

3. RESULTS AND DISCUSSION

3.1. Preferential Binding Sites. In agreement with the conclusions drawn by Nagaki et al.,[23] we find that metal-terminated regions on the surface of MB_6 materials do not contribute toward attractive interactions with hydrogen. The outermost layer of cations are shown to repel molecular hydrogen in the molecular dynamics simulations, and these repulsive interactions are substantial enough to warrant no further analysis of the metal-terminated 1×1 systems in this work. Figure 4 shows sample trajectories for the hydrogen

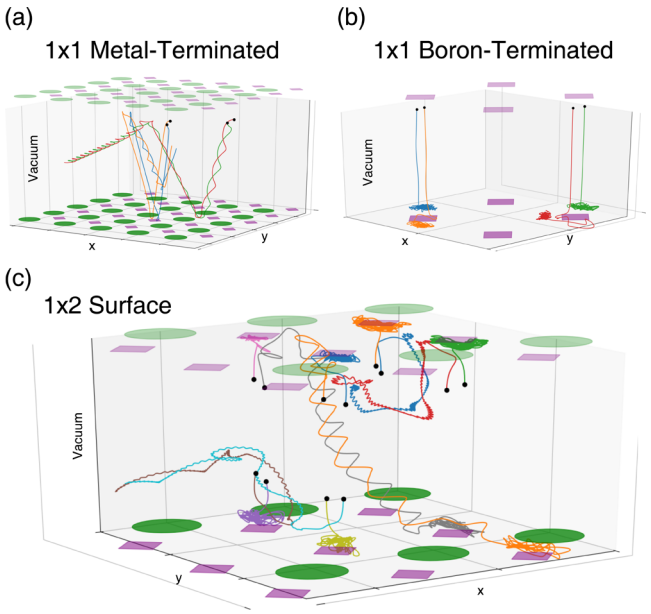

Figure 4. Sample trajectories of hydrogen atoms during the course of CPMD simulations for (a) 1×1 metal-terminated slabs (two hydrogen molecules), (b) 1×1 boron-terminated slabs (two hydrogen molecules), and (c) 1×2 slabs having both metal and boron terminations (six hydrogen molecules). Initial starting points are designated by filled circles for each atom with initial state as molecular hydrogen. MB_6 surfaces at the x–y plane and vacuum in the z-direction, all axes with arbitrary units of length.

atoms obtained from CPMD simulations. The scales on the axis of the figure are arbitrary and are used to summarize the dynamic trajectories of the hydrogen atoms. The x–y plane represents the metal hexaboride surface, and the initial positions of the molecular hydrogen are in the vacuum region in the z-direction. For example, for the case of molecular hydrogen interacting with a metal-terminated surface, Figure 4a shows the trajectory of two hydrogen molecules (four atoms) with initial positions at the black dots (●) moving toward the x–y plane (the surface) with an arbitrary impulse. Notice that the hydrogen molecules bounced back from the surface and become trapped in the vacuum region perpetually rebounding from metal to metal due to the boundary conditions of the supercell.

A reduction in the cation concentration at the surface exposes the octahedra and allows for boron–hydrogen interactions to occur. Figure 4b displays the result of a 1×1 surface composed entirely of boron. The two hydrogen molecules shown are rapidly adsorbed, displaying a degree of migration along the surface for the separate hydrogen atoms clearly splitting from the original equilibrium molecular structure and bond distance. An interesting observation from

DOI: 10.1021/acsomega.8b02652
ACS Omega 2019, 4, 65–72

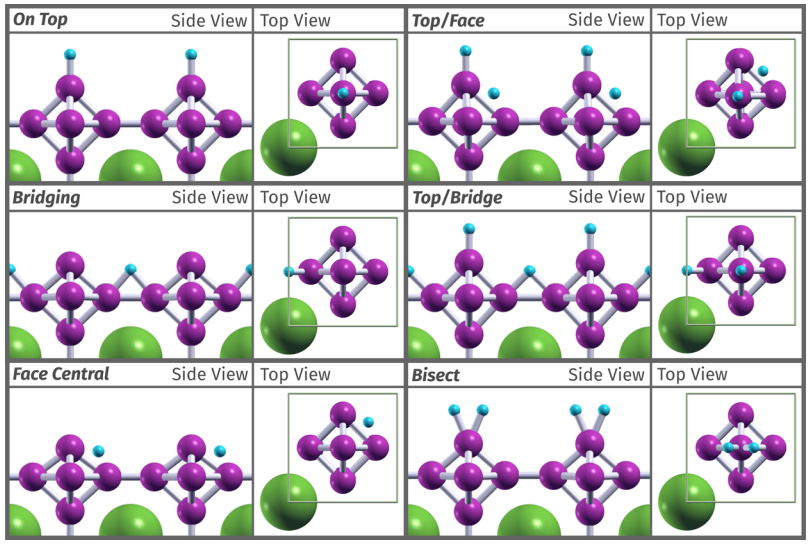

Figure 5. Potential binding locations for a single hydrogen atom (left panel) and molecular hydrogen (right panel) adsorption on metal hexaboride surfaces. Each position is shown for a boron-terminated region on the surface of the slab.

the CPMD is the occurrence of partner exchange with the adsorbed hydrogen atoms. Figure 4c displays the trajectory of six H_2 molecules during the course of the simulation for a CaB_6 1 × 2 slab. Beginning with the initial locations for each atom, indicated by paired black circles, each molecule that binds to the surface results in one atom with a tightly constrained position and the other having translational freedom. The tightly bound hydrogen atoms are typically located in the vicinity of the dangling bond resulting from the cleavage, though some local displacement is also observed. Trajectories of the mobile atoms follow paths which avoid terminal cations on the surface, and recombination/desorption events occur at the intersection of two migrating hydrogens. A similar effect has been observed in studies on boron-doped graphite surfaces. While an increased boron concentration produces larger binding energies for hydrogen, the diffusion barriers and recombination activation energies decrease accordingly.[35] Examination of the CPMD trajectories suggests the method of travel prior to recombination to be along the octahedral face and bridging sites connecting separate unit cells on the surface. The mobile character of adsorbed hydrogen on the facial sites is also seen[36] on the hexahydro-*closo*-hexaborate dianion $[B_6H_6]^{2-}$, which has an analogous structure to the metal hexaborides described in this work. These trajectories show that the chemisorption phenomenon seems to be governing interactions of hydrogen in nonmetal-terminated regions. The accuracy of the trajectories can be improved by incorporating van der Waals effects in the calculations to better describe interactions between nuclei. This work provides enough evidence that the chemisorption phenomenon occurs, where vdW forces are not as relevant than for the case of physisorption or molecular diffusion of hydrogen.

Figure 5 illustrates possible binding locations for single and molecular hydrogen on the surface of boron-terminated hexaborides. The left panel is for binding sites of single hydrogen atoms (three positions, namely, "on-top", "bridging", and "face central", respectively), whereas the right panel describes potential binding sites for two hydrogen atoms or multiatom adsorption. For example, the difference between "on-top" and "top/face" is the addition of the second hydrogen atom at the "face central" position. The most stable adsorption sites for single hydrogen atoms, as evaluated by the residence time in CPMD simulations, are shown on the left portion of Figure 5 for boron-terminated regions of the surfaces. For the case of multiatom adsorption, we have also included the combinations "top/face" and "top/bridge", as shown on the right portion of Figure 5. The "face/bridge" combination is initially included; however, the hydrogen atom located in the face site invariably switches to the top position upon relaxation of the ionic coordinates. An additional configuration in the lower right of Figure 5 named "bisect" is also investigated to compare with the σ complexes associated with metal-catalyzed reactions.[37]

3.2. Geometric Effects. A consequence of hydrogen local dissociation and adsorption on these surfaces is that hydrogen-induced dereconstruction is observed on the terminal octahedra in many cases. While it is typical for the outermost hexaboride unit to contract by 20−25% of the bulk distance along the surface normal,[26] this effect is mitigated with hydrogen chemisorption when atoms located in the "on-top" position are present. Similar dereconstructions caused by hydrogen adsorption have been observed for other materials.[38]

Table 1. Surface Relation Described by $\Delta B_z^{\sigma a}$

slab	surface (σ)	BaB_6	CaB_6	LaB_6	SrB_6
1 × 1	clean	−27.43	−25.01	−19.82	−26.25
	on-top	−1.15	+1.00	−1.18	−0.27
	top/face	−0.69	+1.17	+0.27	+0.23
	top/bridge	−0.88	+0.33	−0.89	−0.24
1 × 2	clean	−10.90	−7.70	+2.04	−9.31
	on-top	−4.96	−2.35	−2.99	−3.90
1 × 4	clean	−28.22	−25.19	−25.31	−26.77
	on-top	−2.73	−0.24	−1.74	−1.37
2 × 2	clean	−10.47	−6.77	+2.33	−8.76
	on-top	−4.92	−1.90	−2.61	−3.65

[a]Relative distances between top and bottom boron atoms located in the first layer for clean and adsorbed surfaces (see eq 1). Only octahedra which have a hydrogen attached in the "on-top" position or their locations on the clean surface are considered here.

DOI: 10.1021/acsomega.8b02652
ACS Omega 2019, 4, 65−72

These expansions are described in Table 1 using the parameter ΔB_z^σ, defined as

$$\Delta B_z^\sigma = \left(\frac{B_{z,\mathrm{top}}^\sigma - B_{z,\mathrm{bot}}^\sigma}{B_{z,\mathrm{top}}^{\mathrm{bulk}} - B_{z,\mathrm{bot}}^{\mathrm{bulk}}} - 1 \right) \times 100\% \quad (1)$$

where $B_{z,\mathrm{pos}}^\sigma$ is the z-coordinate (normal to the surface) of the boron atom in either the top or bottom position (pos) in the first layer of the surface σ. This boron−boron distance is normalized by its bulk equilibrium value

$$B_{z,\mathrm{top}}^{\mathrm{bulk}} - B_{z,\mathrm{bot}}^{\mathrm{bulk}} = a\cdot(1 - 2z) \quad (2)$$

for the lattice constant, a, and positional parameter, z. Aside from the LaB_6 1 × 2 and 2 × 2 slabs, significant expansions are observed upon hydrogen adsorption. One possibility for the strange behavior of LaB_6 is that these surfaces are more stable and thus less likely to accept a hydrogen atom because the 1 × 2 slab results in the lowest surface energy for LaB_6.

For the other cases, it is hypothesized that the increased charge density upon formation of the sigma H−B bond reduces the stress caused by cleavage, placing the affected boron atoms in a more bulk-like environment. Some insight into this effect can be gained by analyzing the bonding charge density. For the reaction

$$(\mathrm{MBA}_6)_{\mathrm{N}_z}^{(\mathrm{s})} + 1/2\mathrm{H}_2^{(\mathrm{g})} \rightleftharpoons \mathrm{H} - (\mathrm{MB}_6)_{\mathrm{N}_z}^{(\mathrm{s})} \quad (3)$$

where N_z is the layer depth through the slab between the top and bottom surfaces, charge densities are calculated for the final relaxed state and the two initial states, resulting in three separate density data sets. The initial coordinates for the clean slab and hydrogen atom are taken from the final relaxed system to allow for direct comparison between the two states. Removal of the initial adsorbate and surface charge densities from the final relaxed geometry produces the bonding charge density. Although this method does not use the geometry of the relaxed clean surface, it does help in producing a qualitative picture of the charge redistribution accompanying adsorption.

The top half of Figure 6a−e shows the calculated bonding charge density resulting from a single hydrogen atom chemisorbed at the "on-top" position of the 1 × 1 CaB_6 surface. The charge densities in Figure 6a−e show positive (red) and negative (blue) isosurfaces of the electron density difference, ranging from the maximum deficit value of ±0.186 electrons Å^{-3}, Figure 6a, down to a lower value of ±0.05 electrons Å^{-3} given in Figure 6e. The obvious increase to the charge density originates just above the terminal boron atom where the hydrogen has become chemisorbed.

Switching to the negative (blue) deviations, density deficits in the form of rings begin to appear in Figure 6b around the terminal boron atom ($B_{z,\mathrm{top}}$). Successive reductions in the density isosurfaces show the diffuse nature of this electron localization on the clean surface lacking bound hydrogen, evidenced by the negative charge density. The bottom portion of Figure 6 points to the origin of these missing rings upon adsorption. Charge density plots for the relaxed 1 × 1 CaB_6 surface are shown in Figure 6f−j for electron densities decreasing from ρ_e = 1.00 Å^{-3} to ρ_e = 0.80 Å^{-3}. In the absence of a suitable hydrogen atom to interact with the affected surface atoms, considerable structural and electronic rearrangement occurs to stabilize the electron-deficient boron atoms. These atoms achieve this stabilization by contracting inward and pulling significant density from the nearest three-center two-electron bonds within the octahedra, though the overall charge displacement can extend much further inward.

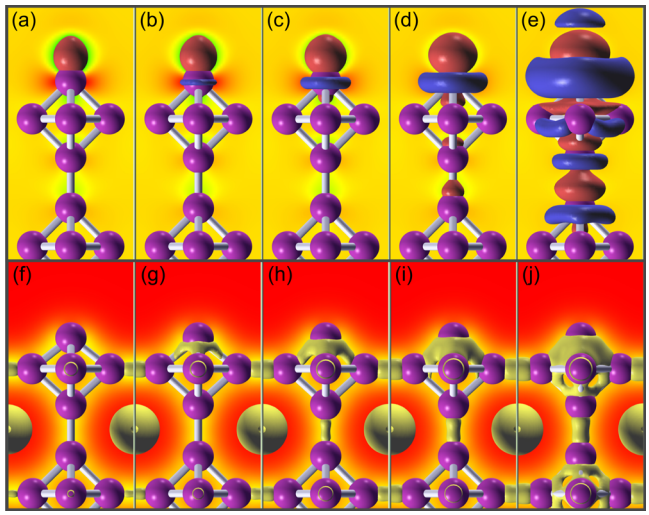

Figure 6. Top: bonding charge density for hydrogen adsorbed in the "on-top" position of a CaB_6 1 × 1 slab. Images show isosurfaces taken at (a) 0.186, (b) 0.150, (c) 0.100, (d) 0.050, and (e) 0.010 Å^{-3}. Positive and negative deviations are shown as red and blue surfaces, respectively. Bottom: charge density isosurfaces for the relaxed 1 × 1 CaB_6 slab for decreasing electron densities of (f) 1.00, (g) 0.95, (h) 0.90, (i) 0.85, and (j) 0.80 Å^{-3}.

Table 2 shows the calculated distances between hydrogen and the nearest boron atom for the "on-top" position. Average distances between hydrogen and the nearest two and three neighbors are also given for the "bridging" and "face" positions. Calculated bond distances for the "on-top" hydrogens qualitatively follow the trends shown in Table 1, in which a smaller and presumably stronger boron−hydrogen bond is accompanied by an expansion of the surface octahedra toward the bulk value. Additionally, for the multiatom bonding on the 1 × 1 slabs, the sigma-B−H bond "on-top" is weakened by the presence of nearby adsorbates, showing the influence of surface coverage.

Table 2. Calculated B−H Bond Distances (Å)[a]

slab	geometry	site	BaB_6	CaB_6	LaB_6	SrB_6
1 × 1	on-top	T	1.1891	1.1886	1.1883	1.1889
	bridging	Br	1.3016	1.2969	1.3194	1.3012
	top/face	T	1.1916	1.1916	1.1910	1.1916
		F	1.4326	1.4249	1.4260	1.4280
	top/bridge	T	1.1907	1.1906	1.1911	1.1909
		Br	1.3036	1.3010	1.3231	1.3018
	bisect	Bi	1.2724	1.2650	1.2268	1.2710
1 × 2	on-top	T	1.2271	1.2219	1.2213	1.2276
	bridging	Br	1.3024	1.2952	1.3155	1.2981
1 × 4	on-top	T	1.1981	1.1951	1.1921	1.1962
	bridging	Br	1.3288	1.3180	1.3349	1.3283
2 × 2	on-top	T	1.2235	1.2149	1.2125	1.2216
	bridging	Br	1.3118	1.3020	1.3314	1.3076

[a]Sites: Bi = bisect, Br = bridging, F = face, T = top.

3.3. Local Adsorption Energies. The calculated adsorption energies for each of the binding geometries considered for 1 × 1 slabs are given in Table 3, where the adsorption energy is given by

DOI: 10.1021/acsomega.8b02652
ACS Omega 2019, 4, 65−72

Table 3. Calculated Local Adsorption Energies for 1 × 1 Slabs (eV/H)[a]

	single hydrogen atom		single hydrogen molecule		
boride	on top	bridging	top/face	top/bridge	bisect
BaB_6	−0.9263	1.1707	−0.8654	−0.6524	−0.3409
CaB_6	−1.1690	1.2594	−0.8912	−0.6720	−0.3689
LaB_6	−2.1940	1.2179	−0.8831	−0.7662	−0.5750
SrB_6	−1.0277	1.2527	−0.8753	−0.6663	−0.3564

[a]Adsorption energies are given per hydrogen atom. Each geometry is displayed in Figure 5.

$$\mathbb{E}^{\sigma}_{ads} = \mathbb{E}^{\sigma}_{ads+slab} - (\mathbb{E}^{\sigma}_{slab} + 1/2\mathbb{E}_{H_2}) \quad (4)$$

where each of the calculations is performed in a supercell having the same dimensions and described by the identical cutoffs and *k*-point grids. The strongest bond by far is found for LaB_6 with hydrogen adsorbed "on-top", having nearly double the stabilization energy than all others. Reduced bond lengths are found for the "on-top" position with "top/face" geometries, described by the energy reduction upon multiatom adsorption. It is also interesting to note that while the "bridging" position by itself is unstable, having hydrogen adsorbed in the "on-top" position actually makes this position favorable. This result supports the conclusion that migrating hydrogen atoms on the surface follow the facial and bridging pathways prior to recombination as these occurrences are observed only after the hydrogen molecule dissociatively desorbs, leaving one atom stuck to the top position. This atom effectively pulls back the octahedral structure to a more bulk-like state or an ideal 1 × 1 supercell. In this case, the region around the "bridging" position becomes more significant in terms of electron density, favoring potentially the adsorption of the second hydrogen atom in a slightly higher electron region as some of the electron density of the boron atom for the "on-top" position is no longer available. For an ideal, unrelaxed, and symmetric 1 × 1 surface configuration, the electron density around the boron atoms where the "on-top" adsorption occurs is higher than around the "bridging" region supporting the addition of the second hydrogen in 1 × 1 supercells once the former has been occupied. Again, the difference in electron density between "on-top" and "bridging" is relatively small for the unrelaxed 1 × 1 configuration. Other supercell configurations do not have the symmetric behavior of the 1 × 1 arrangement, suggesting that a different local distribution of electron density due to geometrical positioning of the boron-terminated atoms making the "on-top" to be generally favorable.

Energetics for the larger 1 × 2, 1 × 4, and 2 × 2 slabs are given in Table 4. Because of the large system sizes, only single-atom adsorption is considered for these slabs. Adsorption in the top position is by far more favorable for these larger slabs than the 1 × 1 surfaces. This may be due to adsorbate−adsorbate interactions because 1 × 1 slabs did not consider coverage less than one monolayer. However, the larger 1 × 4 slabs show decreasing energy, which suggests that the adsorbate interactions are not long-ranged. In contrast to the 1 × 1 slabs, the most stable adsorption is provided by the CaB_6 crystal with the 2 × 2 surface. The top positions are again highly favored, and hydrogen atoms on the bridging sites give rise to positive energies. Unfortunately, multiatom adsorption is not calculated for these larger slabs, though the CPMD trajectories suggest that this bridging site does in fact become accessible when paired with a hydrogen localized on the top position.

3.4. Work Functions. The work function of a material, defined as the minimum energy required to remove an electron from the material at $T = 0$ K,[39] can be determined from the difference of the electrostatic potential energy in the vacuum, E_{vac}, and the Fermi energy of the slab, E_F, using

$$\Phi = E_{vac} - E_F \quad (5)$$

for a sufficiently large slab, where "bulk"-like properties are prevalent. In this work, planar averages are taken along the direction normal to the surface to determine the vacuum potential and this is used along with the Fermi energy of the slabs to calculate Φ. Work functions are known to be heavily dependent upon the nature of the adsorbed species, as these affect the electrostatic potential and therefore the energy necessary for an electron to escape. In fact, the dipole created by metal-terminated MB_6 materials is one of the main reasons LaB_6 has such a low work function.[40] Additionally, measurements of the work function are proving to be a useful tool to investigate real-time adsorbate surface coverage for some materials.[41] The work functions are calculated for each of the clean and adsorbate-covered surfaces, and these are given in Table 5. Note that work functions for the 1 × 1 slabs are calculated for boron-terminated surfaces and presented to identify general trends. For more accurate calculations, a correction to eq 5 might be necessary because of potential quantum effects in thin-film slabs,[42] by decomposing the work function into separate bulk and surface contributions. All of the surfaces have different electrostatic conditions due the terminations not being the same, which explains some of the variation observed in the calculations.

A general trend observed is that stronger (more negative) adsorption energies yield increased values of the work function for a particular surface. This effect can be related to the stability induced by the adsorption process. Atoms which become chemisorbed to the surface stabilize the cleavage plane through a reduction in the total energy. However, these electrons are effectively localized in space and have energies near the Fermi level. Extracting these from the surface will then

Table 4. Calculated Local Adsorption Energies for Larger Slabs (eV/H)[a]

	on top position			bridging position		
boride	1 × 2	2 × 2	1 × 4	1 × 2	2 × 2	1 × 4
BaB_6	−2.2162	−2.2544	−1.2469	0.4204	0.7511	0.7313
CaB_6	−2.0921	−2.3160	−1.3780	0.4978	0.8608	0.8394
LaB_6	−1.9868	−2.2771	−2.2068	0.7042	1.0434	1.1357
SrB_6	−2.1484	−2.2698	−1.2392	0.4915	0.8327	0.8009

[a]Energies are given per hydrogen atom. Adsorption geometries are shown in Figure 5.

DOI: 10.1021/acsomega.8b02652
ACS Omega 2019, 4, 65−72

Table 5. Calculated Work Functions for Clean and Adsorbate-Covered MB_6 Surfaces (eV)[a]

slab	surface (σ)	BaB_6	CaB_6	LaB_6	SrB_6
1 × 1	clean	4.751	4.441	3.931	4.745
	on-top	6.746	6.662	6.276	6.715
	bridging	4.210	4.573	4.955	4.474
	top/face	5.378	5.016	4.096	5.109
	top/bridge	6.006	5.203	4.705	5.450
	bisect	2.493	1.924	4.277	2.036
1 × 2	clean	3.078	4.481	3.651	3.988
	on-top	2.531	3.599	2.781	3.036
	bridging	2.766	3.980	3.620	3.369
2 × 2	clean	2.950	4.340	3.412	3.727
	on-top	2.424	3.503	3.130	2.908
	bridging	2.579	3.804	3.384	3.185
1 × 4	clean	3.171	4.460	3.173	3.979
	on-top	3.030	4.056	3.675	3.612
	bridging	2.827	3.819	3.302	3.332

[a]Clean 1 × 1 slabs refer to completely boron-terminated surfaces; cations are present on half of the surface sites for clean 1 × 2, 2 × 2, and 1 × 4 surfaces.

require a substantial increase in energy as noted by the work function.

4. CONCLUDING REMARKS

Using a combination of self-consistent DFT calculations and CPMD analysis, we have calculated the basic energetics and interacting behavior of hydrogen with metal hexaboride surfaces. Energetics results show that the local adsorption of a single hydrogen molecule per surface unit cell (one ML) is possible and hydrogen atoms chemisorbed at the dangling bond position are highly favorable. The additional electron density reduces the stress caused during cleavage, producing surface octahedra which have more regular shapes. Analysis of the CPMD simulations also provides insights into the mechanisms accompanying hydrogen recombination reactions on MB_6 surfaces through dissociative adsorption and the method of travel prior to recombination to be along the octahedral face and bridging sites connecting separate unit cells on the surface.

AUTHOR INFORMATION

Corresponding Author

*E-mail: victor.vasquez@unr.edu. Phone: +7757846060. Fax: +7757844764.

ORCID

Olivia A. Graeve: 0000-0003-3599-0502

Victor R. Vasquez: 0000-0002-6604-8096

Notes

The authors declare no competing financial interest.

ACKNOWLEDGMENTS

Funding support for this work was provided by NSF grant no. 1360561 "SNM: Scalable Manufacturing of Unique Hexaboride Nanomaterials for Advanced Energy Generation and Gas Storage Applications". Some figures were produced with XCrySDen.[43]

REFERENCES

(1) Lafferty, J. M. Boride Cathodes. *J. Appl. Phys.* **1951**, *22*, 299−309.

(2) Yorisaki, T.; Tillekaratne, A.; Ren, Y.; Moriya, Y.; Oshima, C.; Otani, S.; Trenary, M. Adsorption and dissociation of water on LaB_6(100) investigated by surface vibrational spectroscopy. *Surf. Sci.* **2012**, *606*, 247−252.

(3) Yorisaki, T.; Tillekaratne, A.; Ge, Q.; Oshima, C.; Otani, S.; Trenary, M. Probing the properties of the (111) and (100) surfaces of LaB_6 through infrared spectroscopy of adsorbed CO. *Surf. Sci.* **2009**, *603*, 3011−3020.

(4) Kawanowa, H.; Souda, R.; Otani, S.; Ikeuchi, T.; Gotoh, Y.; Stracke, P.; Krischok, S.; Kempter, V. Interaction of O_2 with LaB_6(001) surfaces as studied with MIES and UPS. *Surf. Sci.* **2001**, *482−485*, 250−253.

(5) Lavrenko, V. A.; Glebov, L. A.; Lugovskaya, Y. S.; Frantsevich, I. N. Investigation of high-temperature oxidation of lanthanum hexaboride in oxygen and the effect of internal oxidation on the protective properties of the scale. *Oxid. Met.* **1973**, *7*, 131−139.

(6) Ozcomert, J. S.; Trenary, M. Oxide thermal desorption from the LaB_6(100) surface following reaction with O_2. *Chem. Mater.* **1993**, *5*, 1762−1771.

(7) Yamamoto, N.; Rokuta, E.; Hasegawa, Y.; Nagao, T.; Trenary, M.; Oshima, C.; Otani, S. Oxygen adsorption on LaB_6 (100) and (111) surfaces. *Surf. Sci.* **1996**, *357−358*, 708−711.

(8) Yamamoto, N.; Rokuta, E.; Hasegawa, Y.; Nagao, T.; Trenary, M.; Oshima, C.; Otani, S. Oxygen adsorption sites on the PrB_6 (100) and LaB_6 (100) surfaces. *Surf. Sci.* **1996**, *348*, 133−142.

(9) Igityan, A.; Kafadaryan, Y.; Aghamalyan, N.; Petrosyan, S.; Badalyan, G.; Hovsepyan, R.; Gambaryan, I.; Eganyan, A.; Semerjian, H.; Kuzanyan, A. Structural and electrical characteristics of lanthanum oxide formed on surface of LaB_6 film by annealing. *Thin Solid Films* **2014**, *564*, 415−418.

(10) Klauser, S. J.; Bas, E. B. The interaction of oxygen with LaB_6 single crystal surfaces at elevated temperatures. *Appl. Surf. Sci.* **1979**, *3*, 356−363.

(11) Yorisaki, T.; Tillekaratne, A.; Moriya, Y.; Oshima, C.; Otani, S.; Trenary, M. Vibrational spectroscopy of oxygen on the (100) and (111) surfaces of lanthanum hexaboride. *Surf. Sci.* **2010**, *604*, 1202−1207.

(12) Perkins, C. L.; Trenary, M.; Tanaka, T.; Otani, S. X-ray photoelectron spectroscopy investigation of the initial oxygen adsorption sites on the LaB_6 (100) surface. *Surf. Sci.* **1999**, *423*, L222−L228.

(13) Davis, P. R.; Chambers, S. A. A study of oxygen interaction with a LaB_6 (100) single crystal surface. *Appl. Surf. Sci.* **1981**, *8*, 197−205.

(14) Trenary, M. Surface Science Studies of Metal Hexaborides. *Sci. Technol. Adv. Mater.* **2012**, *13*, 023002.

(15) Schmidt, K. M.; Graeve, O. A.; Vasquez, V. R. Ab initio and Molecular Dynamics-Based Pair Potentials for Lanthanum Hexaboride. *J. Phys. Chem. C* **2015**, *119*, 14288−14296.

(16) Schmidt, K. M.; Buettner, A. B.; Graeve, O. A.; Vasquez, V. R. Interatomic pair potentials from DFT and molecular dynamics for Ca, Ba, and Sr hexaborides. *J. Mater. Chem. C* **2015**, *3*, 8649−8658.

(17) Schmidt, K. M.; Vasquez, V. R. A generalized method for the inversion of cohesive energy curves from isotropic and anisotropic lattice expansions. *Phys. Chem. Chem. Phys.* **2015**, *17*, 23423−23437.

(18) Cahill, J. T.; Alberga, M.; Bahena, J.; Pisano, C.; Borja-Urby, R.; Vasquez, V. R.; Edwards, D.; Misture, S. T.; Graeve, O. A. Phase stability of mixed-cation alkaline-earth hexaborides. *Cryst. Growth Des.* **2017**, *17*, 3450−3461.

(19) Cahill, J. T.; Vasquez, V. R.; Misture, S. T.; Edwards, D.; Graeve, O. A. Effect of Current on Diffusivity in Metal Hexaborides. *ACS Appl. Mater. Interfaces* **2017**, *9*, 37357−37363.

(20) Kanakala, R.; Rojas-George, G.; Graeve, O. A. Unique preparation of hexaboride nanocubes: A first example of boride formation by combustion synthesis. *J. Am. Ceram. Soc.* **2010**, *93*, 3136−3141.

DOI: 10.1021/acsomega.8b02652
ACS Omega 2019, 4, 65−72

(21) Kanakala, R.; Escudero, R.; Rojas-George, G.; Ramisetty, M.; Graeve, O. A. Mechanisms of combustion synthesis and magnetic response of high-surface-area hexaboride compounds. *ACS Appl. Mater. Interfaces* **2011**, *3*, 1093−1100.
(22) Buckingham, J. D. Thermionic emission properties of a lanthanum hexaboride/rhenium cathode. *Br. J. Appl. Phys.* **1965**, *16*, 1821−1832.
(23) Nagaki, T.; Inoue, Y.; Kojima, I.; Yasumori, I. Catalytic activity of lanthanum hexaboride for hydrogen−deuterium equilibration. *J. Phys. Chem.* **1980**, *84*, 1919−1925.
(24) Berrada, A.; Mercurio, J. P.; Etourneau, J.; Alexandre, F.; Theeten, J. B.; Duc, T. M. Thermionic emission properties of LaB_6 and CeB_6 in connection with their surface states, examination by XPS, Auger spectroscopy and the Kelvin method. *Surf. Sci.* **1978**, *72*, 177−188.
(25) Kim, Y.; Reed, D.; Lee, Y.-S.; Shim, J.-H.; Han, H. N.; Book, D.; Cho, Y. W. Hydrogenation reaction of CaH_2−CaB_6−Mg mixture. *J. Alloys Compd.* **2010**, *492*, 597−600.
(26) Schmidt, K. M.; Jaime, O.; Cahill, J. T.; Edwards, D.; Misture, S. T.; Graeve, O. A.; Vasquez, V. R. Surface termination analysis of stoichiometric metal hexaborides: Insights from first-principles and XPS measurements. *Acta Mater.* **2018**, *144*, 187−201.
(27) Denlinger, J. D.; Gweon, G.-H.; Mo, S.-K.; Allen, J. W.; Sarrao, J. L.; Bianchi, A. D.; Fisk, Z. Absence of X-point band overlap in divalent hexaborides and variability of the surface chemical potential. *J. Phys. Soc. Jpn.* **2002**, *71*, 1−4.
(28) Bengtsson, L. Dipole correction for surface supercell calculations. *Phys. Rev. B: Condens. Matter Mater. Phys.* **1999**, *59*, 12301−12304.
(29) Giannozzi, P.; Baroni, S.; Bonini, N.; Calandra, M.; Car, R.; Cavazzoni, C.; Ceresoli, D.; Chiarotti, G. L.; Cococcioni, M.; Dabo, I.; et al. Quantum ESPRESSO: A Modular and Open-Source Software Project for Quantum Simulations of Materials. *J. Phys.: Condens. Matter* **2009**, *21*, 395502.
(30) Perdew, J. P.; Burke, K.; Ernzerhof, M. Generalized gradient approximation made simple. *Phys. Rev. Lett.* **1996**, *77*, 3865−3868.
(31) Monkhorst, H. J.; Pack, J. D. Special points for Brillouin-zone integrations. *Phys. Rev. B: Solid State* **1976**, *13*, 5188−5192.
(32) Marzari, N.; Vanderbilt, D.; De Vita, A.; Payne, M. C. Thermal contraction and disordering of the Al(110) surface. *Phys. Rev. Lett.* **1999**, *82*, 3296−3299.
(33) Vanderbilt, D. Soft self-consistent pseudopotentials in a generalized eigenvalue formalism. *Phys. Rev. B: Condens. Matter Mater. Phys.* **1990**, *41*, 7892−7895.
(34) Car, R.; Parrinello, M. Unified approach for molecular dynamics and density functional theory. *Phys. Rev. Lett.* **1985**, *55*, 2471−2474.
(35) Ferro, Y.; Marinelli, F.; Jelea, A.; Allouche, A. Adsorption, diffusion, and recombination of hydrogen on pure and boron-doped graphite surfaces. *J. Chem. Phys.* **2004**, *120*, 11882−11888.
(36) Preetz, W.; Peters, G. The hexahydro-*closo*-hexaborate dianion $[B_6H_6]^{2-}$ and its derivatives. *Eur. J. Inorg. Chem.* **1999**, *1999*, 1831−1846.
(37) Kubas, G. J. Dihydrogen complexes as prototypes for the coordination chemistry of saturated molecules. *Proc. Natl. Acad. Sci. U.S.A.* **2007**, *104*, 6901−6907.
(38) Ancilotto, F.; Selloni, A. Hydrogen-induced dereconstruction of Si(111)2×1 from first-principles molecular dynamics. *Phys. Rev. Lett.* **1992**, *68*, 2640−2643.
(39) Lang, N. D.; Kohn, W. Theory of metal surfaces: work function. *Phys. Rev. B: Solid State* **1971**, *3*, 1215−1223.
(40) Aono, M.; Oshima, C.; Tanaka, T.; Bannai, E.; Kawai, S. Structure of the LaB_6 (001) Surface Studied by Angle-Resolved XPS and LEED. *J. Appl. Phys.* **1978**, *49*, 2761−2764.
(41) Prashanthi, K.; Hawk, J. E.; McGee, R.; Gaikwad, R.; Thundat, T. In-situ probing of thermal desorption of vapor molecules on a nanowire via work function variance. *Nano Res.* **2016**, *9*, 3334−3345.
(42) Fall, C. J.; Binggeli, N.; Baldereschi, A. Deriving accurate work functions from thin-slab calculations. *J. Phys.: Condens. Matter* **1999**, *11*, 2689−2696.
(43) Kokalj, A. Computer graphics and graphical user interfaces as tools in simulations of matter at the atomic scale. *Comput. Mater. Sci.* **2003**, *28*, 155−168.

DOI: 10.1021/acsomega.8b02652
ACS Omega 2019, 4, 65−72